

Identification of optimal prediction error Thévenin models of Li-ion cells using the MOLI approach

P. Lopes dos Santos*, T-P Azevedo Perdicoúlis[†] and Paulo A. Salgado^{‡ §}

December 20, 2022

1 Introduction

One of the challenges in designing battery management systems is to find a suitable model for its cells. Since it is not possible to guarantee that all cells are the same, it is convenient to estimate these models from data, using system identification algorithms.

This report starts by studying the dependence of OCV on SOC in Section 2. In Section 3, the battery equivalent model when a resistor is added to the circuit is stated. As the discharge data is divided into segments where C_0, R_0 are assumed constant, and therefore SOC is constant, thence is described an LTI identification algorithm to be used to estimate the cell model in each segment. In Section 4, the Randles circuit diffusion model is described. In particular, the Warburg impedance is discussed. Also, after presenting the simplified Randles circuit, is stated an identification algorithm that estimates the parameters of this model. In Section 5, is enunciated an algorithm to identify a Thévenin model of 1st and 2nd order. In Section 6, the performance of the two models described in sections 4 and 5, and its respective identification algorithms, is discussed and compared using an experimental set of data.

2 Open circuit voltage

A Li-Ion cell delivers a voltage at his terminals. If the cell is in open circuit, i.e, if there isn't any circuit connected to the cell, the voltage remains constant. Hence, it can be seen as a voltage source with a certain open-circuit voltage

*P. Lopes dos Santos is with INESC TEC & FEUP, Universidade do Porto, Portugal, pjsantos@fe.up.pt

[†]T-P Azevedo-Perdicoúlis is with ISR—Coimbra & Departamento de Matemática, UTAD, 5001-801 Vila Real, Portugal tazevedo@utad.p

[‡]Paulo A. Salgado is with Departamento de Engenharias, UTAD, 5001-801 Vila Real, Portugal psal@utad.pt

[§]FCT - Fundação para a Ciência e a Tecnologia under project: (i) UIDB/50014/2020 for the first author. (ii) UIDB/00048/2020 for the second author. (iii) UIDB/04033/2020 for the third author.

(OCV). It is known that the OCV of a fully charged cell is generally higher than the OCV of a discharged one. This can be included in the model by using a voltage source controlled by the state of charge (SOC) of the cell. The SOC is a dimensionless quantity that is 100% (or 1) when the cell is fully charged and is 0% (or 0) when it is fully discharged. It is defined as

$$SOC(t) = \frac{Q_{max} - q_d(t)}{Q_{max}} \times 100\% = \left(1 - \frac{q_d(t)}{Q_{max}}\right) \times 100\%, \quad (1)$$

where Q_{max} is the maximum charge the cell can store (cell capacity) and $q_d(t)$ is the charge removed from the cell. The OCV is a function of SOC and it is monotonous crescent as it can be seen in Figure 1. If the cell is discharging,

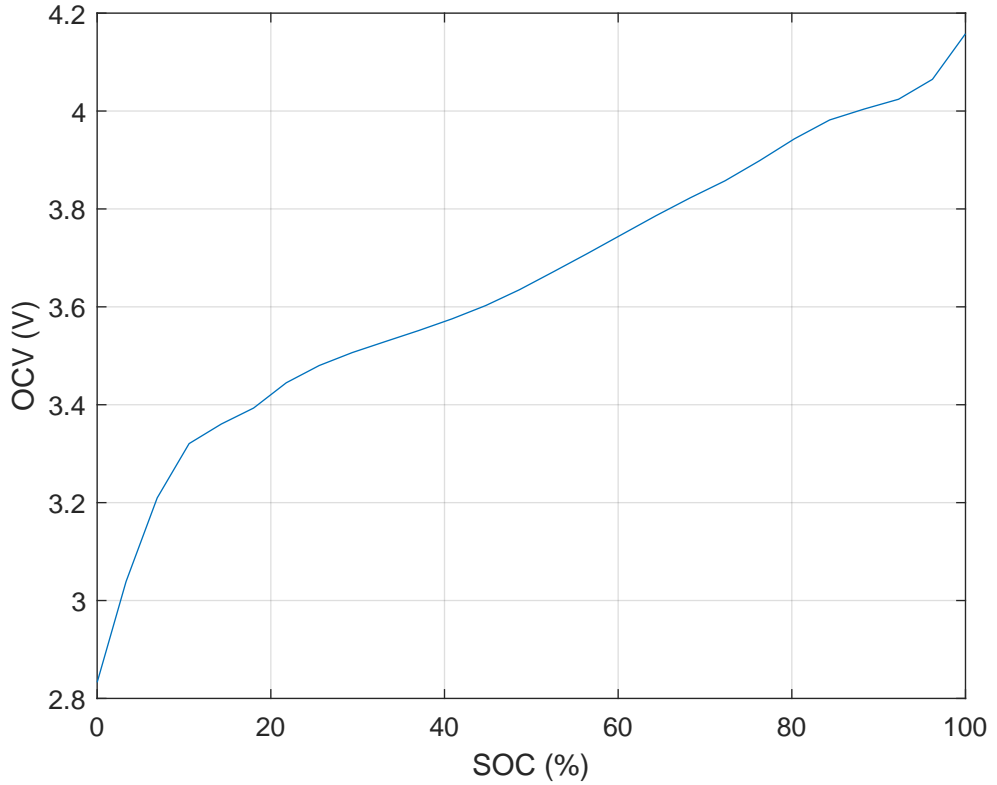


Figure 1: OCV as a function of the SOC

$q_d(t)$ is given by

$$\dot{q}_d(t) = i_{bat}(t), \quad (2)$$

where $i_{bat}(t)$ is the discharge current. If, at time instant t , an infinitesimal amount of charge $dq_d(t)$ is removed from the cell, the voltage at its terminals decreases by an amount of $dOCV(t)$, proporcional to $dq_d(t)$. Thus, we can write

$$dOCV(t) = -\frac{1}{C_0(t)} dq_d(t). \quad (3)$$

Dividing this equation by dt

$$\frac{dOCV(t)}{dt} = -\frac{1}{C_0(t)} \frac{dq_d(t)}{dt} = -\frac{1}{C_0(t)} i_{bat}(t), \quad (4)$$

then the OCV can be seen as the voltage at the terminals of a time varying capacitor as depicted in Figure 2. From equation (3)

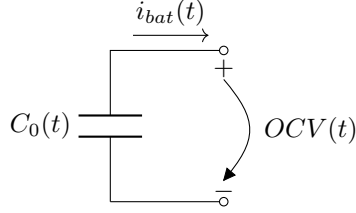


Figure 2: OCV as the voltage at the terminals of a time varying capacitor

$$\frac{dOCV}{dq_d} = -\frac{1}{C_0}. \quad (5)$$

On the other hand, from (1),

$$dq_d = -\frac{Q_{max}}{100} dSOC \quad (6)$$

whereby

$$\frac{dOCV}{dSOC} = \frac{Q_{max}}{100C_0}. \quad (7)$$

Therefore, from Figure 1 we see that C_0 is a function of the SOC, i.e., $C_0 = C_0(SOC)$.

3 Battery equivalent series resistance model

When a load is connected to the cell, its voltage drops. This can be modelled by a resistor in series with the capacitor as shown in Figure 3. This is the series

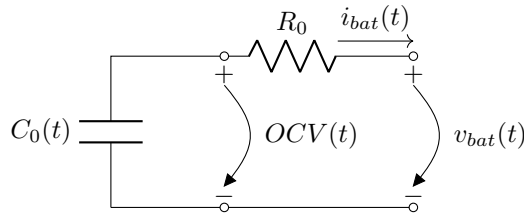


Figure 3: Equivalent series resistance model

resistance equivalent (SRE) model. With the SRE, recalling (4) and knowing

that OCV depends on SOC, the cell model becomes

$$OCV(t) = -\frac{1}{C_0(SOC)}i_{bat}(t), \quad (8)$$

$$v_{bat}(t) = OCV(t) - R_0i_{bat}(t), \quad (9)$$

where v_{bat} is the voltage at the cell terminals. This can be seen as a continuous-time, quasi LPV state-space model:

$$\dot{x}(t) = A_c x(t) + B_c(p_t)u(t), \quad (10)$$

$$y(t) = Cx(t) + Du(t), \quad (11)$$

with input $u(t) = i_{bat}(t)$, output $y(t) = v_{bat}(t)$, scheduling signal $p_t = SOC(t)$ and parameters $A_c = 0$, $B_c(t) = -\frac{1}{C_0(t)}$, $C = 1$ and $D = -R_0$. In discrete-time, assuming that $i_{bat}(t)$ and $SOC(t)$ are constant between samples (ZOH digital to analog converters), the equivalent cell model is

$$OCV[k+1] = OCV[k] - \frac{T_s}{C_0(p_k)}i_{bat}[k] \quad (12)$$

$$v_{bat}[k] = OCV[k] - R_0i_{bat}[k]. \quad (13)$$

Also, from (2) and (1),

$$q_d[k+1] = q_d[k] + T_s i_{bat}[k] \quad (14)$$

$$p_k = SOC[k] = \left(1 - \frac{q_d[k]}{Q_{max}}\right) 100. \quad (15)$$

When $k = 0$, (15) becomes:

$$q_d[0] = \left(1 - \frac{SOC[0]}{100}\right) Q_{max}. \quad (16)$$

Note that R_o is often a function of SOC and always a function of the temperature. In what follows, we assume constant temperature and that both R_0 and C_0 are piecewise constant functions of SOC. Consequently, these parameters remain constant in the time intervals where both C_0 and R_0 are constant (that is, the intervals where SOC is constant). For this reason, in each one of these intervals — hereforth called segments — the cell model is time invariant. So, to identify the piecewise LTI model, the discharge data is divided into several segments, where every segment- i has N_i data points. For each segment, an LTI identification algorithm is used with the OCV initial value being the final of the previous one (except for the first one where the initial OCV also needs to be estimated).

3.1 Identification of the series resistance model

We derive the LTI identification algorithm that will be used to identify the cell model in each segment- i containing N_i data points. Using the shift forward operator z , i.e., $zx[k] = x[k+1]$, and considering $C_0(p_k) = C_{0_i} = \text{constant}$, equation (12) may be written as

$$OCV[k] = -\frac{T_s}{C_{0_i}} \frac{i_{bat}[k]}{z-1}. \quad (17)$$

But, from (14),

$$T_s \frac{i_{bat}[k]}{z-1} = q_d[k]. \quad (18)$$

Consequently,

$$OCV[k] = OCV[0] - \frac{1}{C_{0_i}} q_d[k], \quad (19)$$

and, substituting (19) into (13),

$$y[k] := v_{bat}[k] = OCV[0] - \frac{1}{C_{0_i}} q_d[k] - R_{0_i} i_{bat}[k]. \quad (20)$$

In the first segment, i.e, if $i = 1$, define:

$$\varphi_1[k] := [1 \quad -q_d[k] \quad -i_{bat}[k]] \quad (21)$$

where $q_s[k]$ is given by (14) with $q_d[0] = 0$, and

$$\theta_1 := \left[OCV[0] \quad \frac{1}{C_{0_1}} \quad R_{0_1} \right]^T, \quad (22)$$

and using (21) and (22) rewrite (20) as:

$$y[k] = \varphi_i[k] \theta_i, \quad (23)$$

with $i = 1$. Given $y[k]$ and $i_{bat}[k]$ for $k = 0, \dots, N_1 - 1$, the LSE of θ_1 is calculated as:

$$\hat{\theta}_i = (\Phi_i^T \Phi_i)^{-1} \Phi_i^T Y_i \quad (24)$$

with $i = 1$, and

$$\Phi_i := [\varphi[0]^T \quad \varphi[1]^T \quad \dots \quad \varphi[N-1]^T]^T, \quad (25)$$

$$Y_i := [y[0] \quad y[1] \quad \dots \quad y[N_i-1]]^T. \quad (26)$$

In any other segment, i.e., $i = 2, \dots$, define $k' = k - \sum_{j=1}^{i-1} N_j + 1$ and rewrite (20) as

$$y[k'] := v_{bat}[k'] - OCV[k' = 0] = -\frac{1}{C_{0_i}} q_d[k'] - R_{0_i} i_{bat}[k'], \quad (27)$$

with $OCV[k' = 0] = OCV \left[\sum_{j=1}^{i-1} N_j - 1 \right]$. This equation can also be rewritten as (23) with k replaced by k' and

$$\varphi_i[k'] := [-q_d[k'] \quad -i_{bat}[k']], \quad (28)$$

$$\theta_i := \left[\frac{1}{C_{0_1}} \quad R_{0_1} \right]^T, \quad (29)$$

with the estimate of θ_i still being given by (24).

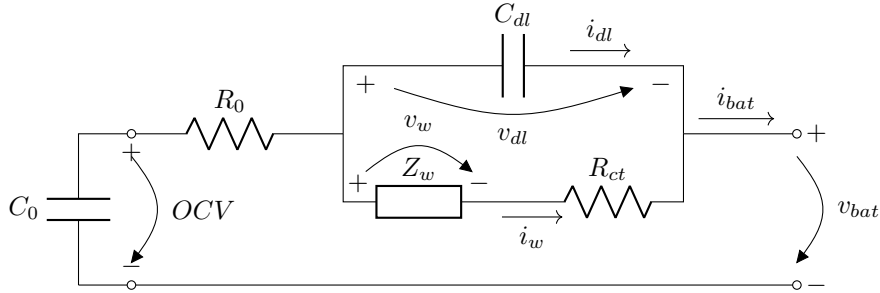


Figure 4: Randles' circuit

4 Randles circuit diffusion model

Cells are often modelled by the Randles circuit depicted in Figure 4. This circuit is inspired by electrochemical principles and it is recognised to be a trusty description of a cell dynamics [16].

Here, R_0 is the electrolyte resistance, R_{ct} is the charge transfer resistance that models the voltage drop over the electrode–electrolyte interface due to a load, C_{dl} is the double-layer capacitance modelling the effect of charges building up in the electrolyte at the electrode surface, and Z_W is the so called Warburg impedance. The main difficulty is to model the Warburg impedance.

Next, the Warburg impedance is described and discretised to be next approximated by a finite state-space realization. To identify the parameters of the simplified Randles circuit, a MOLI like identification algorithm is formulated.

4.1 Warburg impedance

The Warburg impedance models the diffusion of lithium ions in the electrodes. It is a frequency dependent impedance, given by

$$Z_w = \frac{A_w}{\sqrt{j\omega}}, \quad (30)$$

where $j = \sqrt{-1}$ is the imaginary unity, A_W is the Warburg coefficient, and ω is the frequency in radians per second. Figure 5 shows the Bode diagrams of Z_w , where it can be seen that the amplitude diagram is a straight line with a slope of -10 dB per decade, and the Phase constant and equal to -45° .

4.1.1 Fractional integrator

The Warburg impedance is a semi-integrator of the current. The semi-integrator is a special case of the fractional integrator of order α with transfer function $\frac{1}{s^\alpha}$. It is well known that the inverse Laplace transform of $\frac{1}{s^n}$ is zero for $t < 0$ and

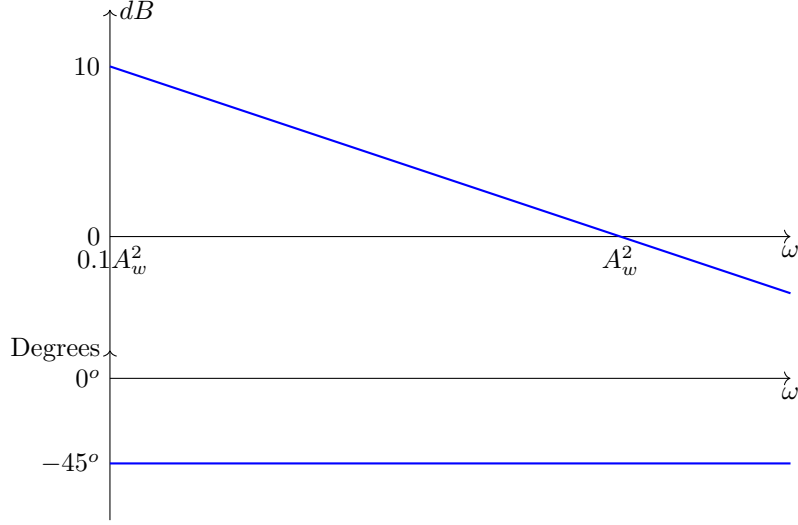


Figure 5: Bode diagrams of the Warburg impedance

$\frac{t^{n-1}}{(n-1)!}$ for $t \geq 0$, i.e.,

$$\mathcal{L}^{-1} \left\{ \frac{1}{s^n} \right\} = \begin{cases} 0, & t < 0 \\ \frac{t^{n-1}}{(n-1)!}, & t \geq 0 \end{cases} = \frac{t^{n-1}}{\Gamma(n)} \mathbf{1}(t), \quad (31)$$

where $\mathbf{1}(t)$ is the unit step. As for any positive integer n the Gamma function is given by,

$$\Gamma(n) = \int_0^{\infty} x^{n-1} e^{-x} dx = (n-1)!, \quad (32)$$

then

$$\mathcal{L}^{-1} \left\{ \frac{1}{s^n} \right\} = \begin{cases} 0, & t < 0 \\ \frac{t^{n-1}}{\Gamma(n)}, & t \geq 0 \end{cases} = \frac{t^{n-1}}{\Gamma(n)} \mathbf{1}(t). \quad (33)$$

Generalizing this result for $\mathcal{L}^{-1} \left\{ \frac{1}{s^\alpha} \right\}$, with $\alpha \in \mathbb{R}^+$, yields,

$$\mathcal{L}^{-1} \left\{ \frac{1}{s^\alpha} \right\} = \begin{cases} 0, & t < 0 \\ \frac{t^{\alpha-1}}{\Gamma(\alpha)}, & t \geq 0 \end{cases} = \frac{t^{\alpha-1}}{\Gamma(\alpha)} \mathbf{1}(t). \quad (34)$$

This relation can be confirmed by the calculation of $\mathcal{L} \{ t^{\alpha-1} \mathbf{1}(t) \}$:

$$\mathcal{L} \{ t^{\alpha-1} \mathbf{1}(t) \} = \int_0^{\infty} t^{\alpha-1} e^{-st} dt = \int_0^{\infty} \frac{u^{\alpha-1}}{s^{\alpha-1}} e^{-st} \frac{du}{s} = \frac{1}{s^\alpha} \int_0^{\infty} u^{\alpha-1} e^{-u} du = \frac{\Gamma(\alpha)}{s^\alpha}. \quad (35)$$

Therefore,

$$\mathcal{L} \left\{ \frac{t^{\alpha-1} \mathbf{1}(t)}{\Gamma(\alpha)} \right\} = \frac{1}{s^\alpha} \Leftrightarrow \mathcal{L}^{-1} \left\{ \frac{1}{s^\alpha} \right\} = \frac{t^{\alpha-1}}{\Gamma(\alpha)} \mathbf{1}(t). \quad (36)$$

4.2 Impulse response of the sampled Warburg impedance

The system is sampled with a Zero Order Hold (ZOH) to obtain the discrete time system, followed by its rational approximation.

4.2.1 Zero Order Hold sampling

The output of a fractional integrator is

$$y(t) = \int_{\tau=0}^{\infty} \frac{\tau^{\alpha-1}}{\Gamma(\alpha)} u(t-\tau) d\tau. \quad (37)$$

If $u(t)$ is the output of a ZOH system (p.e, a DA converter), then it is constant between to consecutive sampling instants, i.e.,

$$u(t) = u(kT_s) = u[k], kT_s \leq t < (k+1)T_s, \quad (38)$$

where T_s is the sampling period. For this input, the output at the sampling instant $t = kT_s$ is

$$\begin{aligned} y(kT_s) &= y[k] = \frac{1}{\Gamma(\alpha)} \sum_{\ell=1}^{\infty} \int_{(\ell-1)T_s}^{\ell T_s} \tau^{\alpha-1} u[k-\ell] d\tau \\ &= \frac{1}{\alpha \Gamma(\alpha)} \sum_{\ell=1}^{\infty} [\tau^\alpha]_{\tau=(\ell-1)T_s}^{\ell T_s} u[k-\ell] = \sum_{\ell=1}^{\infty} \frac{(\ell T_s)^\alpha - ((\ell-1)T_s)^\alpha}{\alpha \Gamma(\alpha)} u[k-\ell] \\ &= \frac{T_s^\alpha}{\alpha \Gamma(\alpha)} \sum_{\ell=1}^{\infty} (\ell^\alpha - (\ell-1)^\alpha) u[k-\ell] = \frac{T_s^\alpha}{\alpha \Gamma(\alpha)} (h[k] * u[k]), \end{aligned}$$

where $*$ stands for convolution and

$$h[k] = k^\alpha - (k-1)^\alpha, \quad k = 1, 2, \dots, \infty. \quad (39)$$

Hence, the impulse response of the fractional integrator is

$$h[k] = \begin{cases} 0, & k < 1 \\ \frac{T_s^\alpha}{\alpha \Gamma(\alpha)} (k^\alpha - (k-1)^\alpha), & k \geq 1 \end{cases} = \frac{T_s^\alpha}{\alpha \Gamma(\alpha)} ((k+1)^\alpha - k^\alpha) \mathbf{1}[k-1], \quad (40)$$

where $\mathbf{1}[k]$ is the discrete-time unit step. As the Warburg impedance is a fractional integrator with $\alpha = 0.5$, its impulse response is

$$\begin{aligned} w[k] &= \begin{cases} 0, & k < 1 \\ \frac{2A_w \sqrt{T_s}}{\Gamma(0.5)} (\sqrt{k} - \sqrt{k-1}), & k \geq 1 \end{cases} \\ &= \frac{2A_w \omega \sqrt{T_s}}{\Gamma(0.5)} (\sqrt{k} - \sqrt{k-1}) \mathbf{1}[k-1] \end{aligned} \quad (41)$$

$$= 1.1284 A_w \sqrt{T_s} (\sqrt{k} - \sqrt{k-1}). \quad (42)$$

Figure 6 shows the normalised impulse response of the Warburg impedance, $\frac{w[k]}{A_w \sqrt{T_s}}$.

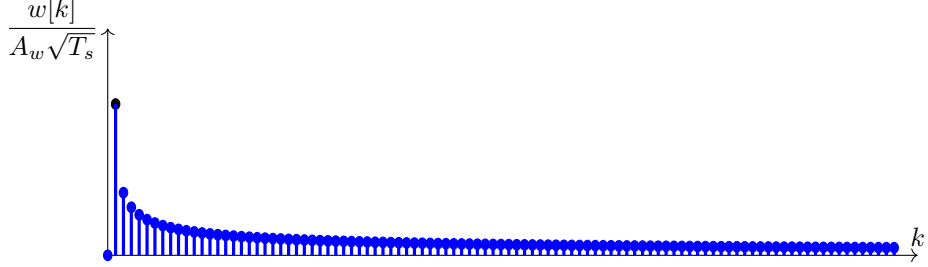


Figure 6: Normalized Discrete-time impulse response of the Warburg Impedance

4.2.2 Rational approximation of the Warburg impedance

The discrete-time normalized Warburg impedance $\frac{Z_w}{A_w \sqrt{T_s}}$ was approximated by the following state-space realization of a rational transfer function using the Ho-Kalman algorithm.

$$x_w[k+1] = A_z x_w[k] + B_z i_w[k] \quad (43)$$

$$y_w[k] = C_z x_w[k] \quad (44)$$

with

$$A_z = \begin{bmatrix} 0.99964 & -0.0014121 & -0.0025413 & -0.0028264 & -0.0012488 & 0.00041095 & 0.00012636 \\ -0.0014120 & 0.98934 & -0.028798 & -0.036660 & -0.018323 & 0.0065444 & 0.0023842 \\ -0.0025412 & -0.028798 & 0.88467 & -0.18947 & -0.11661 & 0.051034 & 0.021731 \\ -0.0028263 & -0.036660 & -0.18947 & 0.61030 & -0.30015 & 0.16198 & 0.080232 \\ -0.0012488 & -0.018323 & -0.11661 & -0.30015 & 0.70033 & 0.21261 & 0.12742 \\ 0.00041094 & 0.0065444 & 0.051034 & 0.16198 & 0.21261 & 0.78626 & -0.17239 \\ 0.00012635 & 0.0023842 & 0.021731 & 0.080232 & 0.12742 & -0.17239 & 0.80393 \end{bmatrix} \quad (45)$$

$$B_z = [0.194140 \quad 0.376185 \quad 0.631849 \quad 0.673511 \quad 0.294717 \quad -0.092444 \quad -0.029057]^T \quad (46)$$

$$C_z = [0.194143 \quad 0.376185 \quad 0.631849 \quad 0.673511 \quad 0.294717 \quad -0.092444 \quad -0.029057] \quad (47)$$

This approximation has a relative error of

$$E_{10000} = 0.45\%, \quad (48)$$

where

$$E_T = e_{T_{rms}} / w_{T_{rms}} * 100\%, \quad (49)$$

with $e_{T_{rms}}$ and $w_{T_{rms}}$ being the rms values of

$$e[0:T] = w[0:T] - \hat{w}[0:T] \quad (50)$$

and $w_{0:T}$. Here, $w_{0:T}$ and $\hat{w}_{0:T}$ are vectors with the samples for $k = 0$ to $k = T$ of the impulse responses $w[k]$ and $\hat{w}[k]$ of the Warburg impedance and

its rational approximation, respectively. In Figure 7, it cannot be seen any difference between the impulse responses of the Warburg impedance and its rational approximation because they completely overlap. Figure 8 compares

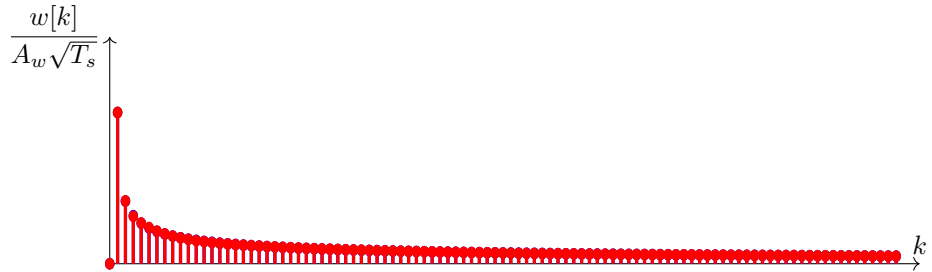


Figure 7: Discrete-time impulse responses of the Warburg Impedance (in blue) and its rational approximation (in red)

the Bode plots where it can be seen that the match is almost perfect up to a frequency of $0.02\omega_N$ where ω_n is the Nyquist frequency. The continuous

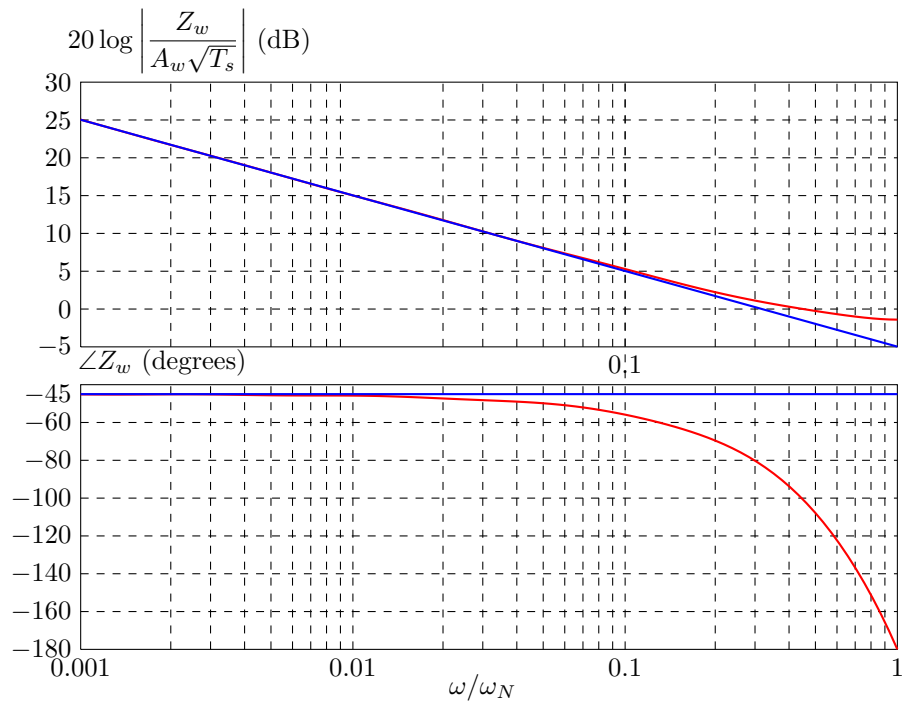


Figure 8: Bode plots the Warburg Impedance (in blue) and its rational approximation (in red)

time rational approximations of Warburg impedance can be derived from this

discrete-time approximation, being equal to

$$\bar{A}_z = \frac{1}{T_s} \ln(A_z) = \quad (51)$$

$$\begin{bmatrix} -0.3835 & -1.7084 & -4.0692 & -6.1460 & -4.1516 & 2.3824 & 1.3965 \\ -1.7082 & -14.4359 & -48.5062 & -79.8499 & -56.4056 & 32.6265 & 19.2953 \\ -4.0691 & -48.5062 & -219.8206 & -421.5413 & -324.2213 & 195.5203 & 116.6362 \\ -6.1458 & -79.8499 & -421.5413 & -911.8301 & -774.4758 & 498.2598 & 304.6979 \\ -4.1515 & -56.4056 & -324.2213 & -774.4758 & -739.1521 & 532.3045 & 345.9606 \\ 2.3823 & 32.6265 & 195.5203 & 498.2598 & 532.3045 & -454.9094 & -343.3191 \\ 1.3964 & 19.2953 & 116.6362 & 304.6979 & 345.9606 & -343.3191 & -321.9213 \end{bmatrix} \frac{10^{-3}}{T_s}$$

$$\bar{B}_z = -(I - A_z)^{-1} \bar{A}_z B_z = \quad (52)$$

$$= \frac{1}{T_s} [0.1881 \quad 0.4215 \quad 0.9410 \quad 1.3845 \quad 0.9325 \quad -0.53116 \quad -0.3131]$$

$$\bar{C}_z = C_w = \quad (53)$$

$$= [0.194143 \quad 0.376185 \quad 0.631849 \quad 0.673511 \quad 0.294717 \quad -0.092444 \quad -0.029057].$$

Figure 9 compares the Bode plots of Z_w and its continuous-time rational approximation. The match is almost perfect for two decades ($10^{-4}/T_s < \omega < 1/T_s$).

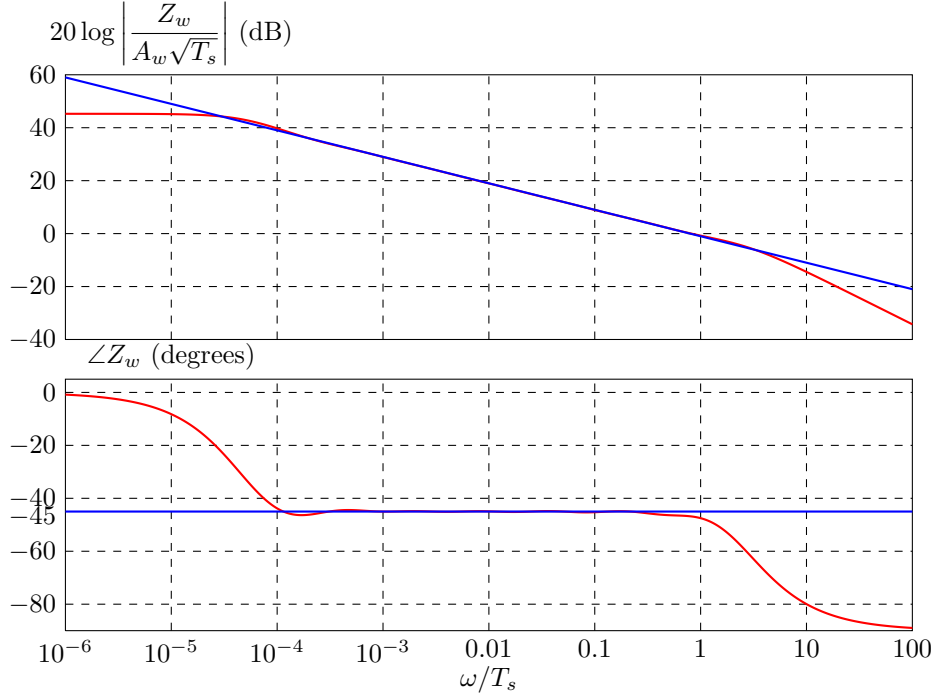


Figure 9: Bode plots the Warburg Impedance (in blue) and its continuous-time rational approximation (in red)

4.3 Identification of the Randles' circuit parameters

Usually, this impedance is approximated by several series of RC parallel circuits, leading to the battery equivalent circuit depicted in Figure 10. It was seen in

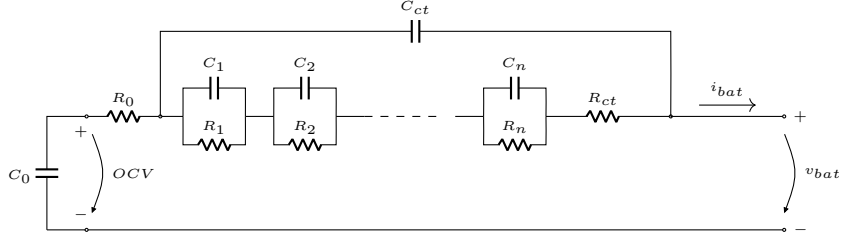


Figure 10: High order approximation of the Warburg impedance

the previous section that the Warburg impedance can be approximated by a 7th order LTI system which means that the circuit in Figure 10 must have at least 7 RC parallels to achieve this approximation, i.e. n must be set to 7 and a naive approach leads to a dynamic system with 17 parameters to be identified. But the approximation of the Warburg impedance, derived in the previous section, has only one unknown parameter. Therefore, using this approximation as a priori knowledge reduces the number of unknown parameters to five: C_0 , C_{ct} , R_o , R_{ct} and A_w . This number can be further reduced to three, since often the double layer capacitance, C_{ct} , is negligible, and when this happens, the charge transfer resistance, R_{ct} , and the electrolyte resistance, R_o , are joined into a single resistance equal to $R_{ct} + R_o$.

In this section an algorithm is formulated to estimate the parameters of the simplified Randles' circuits (without the double layer capacitance).

In a similar manner to Subsection 3.1, this algorithm do not assume variability in the parameters. Instead, it is used in several segments of the discharge processes to estimate a piecewise LTI model.

4.3.1 Simplified Randles' circuit

The simplified Randles' circuit depicted in Figure 11 is approximated by the

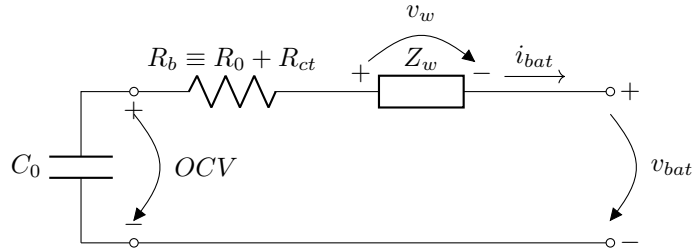


Figure 11: Simplified Randles' circuit

following equations

$$OCV(t) = -\frac{1}{C_0}i_{bat}(t), \quad (54)$$

$$\dot{x}_w(t) = \bar{A}_z x_w(t) + \bar{B}_z i_{bat}(t), \quad (55)$$

$$v_{bat}(t) = OCV(t) - A_w \sqrt{T_s} \bar{C}_z x_w(t) - R_b i_{bat}(t), \quad (56)$$

where A_w is the Warburg coefficient and $(\bar{A}_z, \bar{B}_z, A_w \bar{C}_z)$ is a realisation of a continuous-time approximation of the Warburg impedance. The correspondent ZOH discrete-time model is

$$OCV[k+1] = OCV[k] - \frac{T_s}{C_0} i_{bat}[k], \quad (57)$$

$$x_w[k+1] = A_z x_w[k] + B_z i_{bat}[k], \quad (58)$$

$$v_{bat}[k] = OCV[k] - A_w \sqrt{T_s} C_z x_w[k] - R_b i_{bat}[k], \quad (59)$$

where T_s is the sampling period and $(A_z, B_z, A_w \sqrt{T_s} C_w, 0)$ is the discrete-time realization of the Warburg matrices with A_z , B_z and C_z given in equations (45)-(47). Equation (57) yields (12), that is:

$$OCV[k] = OCV[0] - \frac{T_s}{C_0} \sum_{\tau=0}^k i_{bat}[\tau] = OCV[0] - \frac{1}{C_0} q_d[k]. \quad (60)$$

On the other hand, using the forward time shift operator in equation (58)

$$x_w[k] = (zI - A_z)^{-1} B_z i_{bat}[k] = A_z^k x_w[0] + x_{w0}[k], \quad (61)$$

where $x_{w0}[k]$ is the state the output of the system (A_z, B_z, I) driven by $i_{bat}[k]$ with zero initial state. Using (60) and (61) in (59), the following regressor is obtained for $i = 1$

$$\begin{aligned} y[k] := v_{bat}[k] &= OCV[0] - C_z A_z^k x_w[0] \sqrt{T_s} A_w - q_d[k] \frac{1}{C_0} \\ &\quad - C_z x_{w0}[k] \sqrt{T_s} A_w - R_b i_{bat}[k] \\ &= [1 \quad -C_z A_z^k \quad -q_d[k] \quad -C_z x_{w0}[k] \quad i_{bat}] \begin{bmatrix} OCV[0] \\ \sqrt{T_s} A_w x_w[0] \\ \frac{1}{C_0} \\ \sqrt{T_s} A_w \\ R_b \end{bmatrix} \\ &= \varphi_1[k] \theta_1 \end{aligned}$$

where

$$\varphi_1[k] := [1 \quad -C_z A_z^k \quad -q_d[k] \quad -C_z x_{w0}[k] \quad i_{bat}] \quad (62)$$

$$\theta_1 := \left[OCV[0] \quad \sqrt{T_s} A_w x_w[0] \quad \frac{1}{C_0} \quad \sqrt{T_s} A_w \quad R_b \right]^T. \quad (63)$$

In a similar manner as in Subsection 3.1, for $i = 2, \dots$ we have:

$$\begin{aligned}
y[k] &:= v_{bat}[k] - OCV[0] \\
&= -q_d[k] \frac{1}{C_0} - (C_z A_z^k x_w[0] + C_z x_{w0}[k]) \sqrt{T_s} A_w - R_b i_{bat}[k] \\
&= [-q_d[k] \quad -C_z A_z^k - C_z x_{w0}[k] \quad i_{bat}] \begin{bmatrix} \frac{1}{C_0} \\ \sqrt{T_s} A_w \\ R_b \end{bmatrix}
\end{aligned} \tag{64}$$

$$= \varphi_i[k] \theta_i, \tag{65}$$

where

$$\varphi_i[k] := [-q_d[k] \quad -C_z A_z^k - C_z x_{w0}[k] \quad i_{bat}], \tag{67}$$

$$\theta_i := \begin{bmatrix} \frac{1}{C_0} \\ \sqrt{T_s} A_w \\ R_b \end{bmatrix}^T. \tag{68}$$

Defining

$$Y_i := [y[0] \quad y[1] \quad \dots \quad y[N_i - 1]]^T, \quad i = 1, 2, \dots \tag{69}$$

$$\Phi_i := [\varphi_i[0]^T \quad \varphi_i[1]^T \quad \dots \quad \varphi_i[N_i - 1]^T]^T, \quad i = 1, 2, \dots \tag{70}$$

then

$$Y_i = \Phi_i \theta_i, \tag{71}$$

and if Φ_i is a full rank matrix, θ can be estimated by the LSE:

$$\hat{\theta}_i = \Phi_i^\dagger Y_i = (\Phi_i^T \Phi_i)^{-1} \Phi_i^T Y_i. \tag{72}$$

5 The Modified Thévenin Difusion model

In this section the battery is modelled by the circuit of Figure 12, which can be

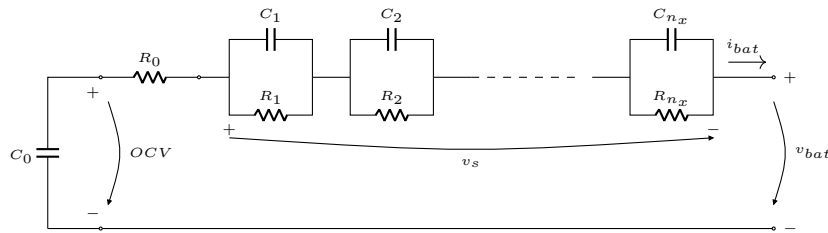


Figure 12: High order equivalent circuit

described by the state-space model

$$\dot{OCV}(t) = -\frac{1}{C_0} i_{bat}(t), \tag{73}$$

$$\dot{x}(t) = A_c x(t) + B_c i_{bat}(t), \tag{74}$$

$$v_{bat}(t) = OCV(t) - Cx(t) - R_o i_{bat}(t), \tag{75}$$

where

$$\dot{x}(t) = A_c x(t) + B_c i_{bat}(t), \quad (76)$$

$$v_s(t) = Cx(t), \quad (77)$$

describes the series of the RC circuits with input $i_{bat}(t)$, output $v_s(t)$. If we specify the initial value of $OCV(0)$ in equation (75),

$$v_{bat}(t) = OCV(0) - \frac{1}{C_0} q_{out}(t) - Cx - R_0 i_{bat}(t) \quad (78)$$

where

$$\dot{q}_{out}(t) = i_{bat}(t), \quad (79)$$

and define next the extended input

$$u_e(t) = \begin{bmatrix} \mathbf{1}(t) \\ i_{bat}(t) \\ q_{out}(t) \end{bmatrix}, \quad (80)$$

with $\mathbf{1}(t)$ being the continuous-time unit step, we can rewrite (74) and (78) as

$$\dot{x}(t) = A_c x(t) + B_{ce} u_e(t) \quad (81)$$

$$v_{bat}(t) = Cx(t) + D_e u_e(t) \quad (82)$$

where some matrices need to be redefined:

$$B_{ce} := [0_n \quad 0_n \quad B_c], \quad D_e := \begin{bmatrix} OCV(0) & -\frac{1}{C_0} & -R_0 \end{bmatrix}. \quad (83)$$

The next step is to discretise the system. Then

$$x[k+1] = Ax[k] + B_e u_e[k], \quad (84)$$

$$v_{bat}[k] = Cx[k] + D_e u_e[k], \quad (85)$$

where

$$B_e = [0_n \quad 0_n \quad B], \quad (86)$$

$$u_e[k] = [\mathbf{1}[k] \quad q_{out}[k] \quad i_{bat}[k]]^T \quad (87)$$

and

$$q_{out}[k+1] = q_{out}[k] + T_s i_{bat}[k]. \quad (88)$$

Here T_s is the sampling period.

5.1 Identification algorithm

Since the data has been partitioned into different segments, we identify a piecewise LTI model in every segment in a similar manner as we have done for the other models.

5.1.1 Segment 1 -Unknown initial OCV and initial state

We use a MOLI approach to formulate the identification algorithm, taking into account that both the initial OCV and the initial state are unknown for the first segment. To do this, first partition A as

$$A = A_0 + LC. \quad (89)$$

Then

$$x[k+1] = A_0x[k] + LCx[k] + B_e u_e[k]. \quad (90)$$

From (85),

$$Cx[k] = v_{bat}[k] - D_e u_e[k]. \quad (91)$$

Substituting (91) into (90) becomes:

$$x[k+1] = A_0x[k] + Lv_{bat}[k] + (B_e - LD_e) u_e[k], \quad (92)$$

and consequently

$$x[k] = A_0^k x[0] + (qI - A_0)^{-1} Lv_{bat}[k] + (qI - A_0)^{-1} (B_e - LD_e) u_e[k]. \quad (93)$$

Expanding B_e , D_e and $u_e[k]$,

$$\begin{aligned} x[k] &= A_0^k x[0] + (qI - A_0)^{-1} Lv_{bat}[k] + \\ &\quad + (qI - A_0)^{-1} \left([0_n \quad 0_n \quad B] - L \begin{bmatrix} OCV[0] & -\frac{1}{C_0} & -R_0 \end{bmatrix} \right) \begin{bmatrix} \mathbf{1}[k] \\ q_{out}[k] \\ i_{bat}[k] \end{bmatrix} \\ &= A_0^k x[0] + (qI - A_0)^{-1} Lv_{bat}[k] - (qI - A_0)^{-1} L OCV[0] \mathbf{1}[k] + \\ &\quad + (qI - A_0)^{-1} \frac{L}{C_0} q_{out}[k] + (qI - A_0)^{-1} B_a i_{bat}[k] \end{aligned} \quad (94)$$

with

$$B_a = B + LR_0. \quad (95)$$

Then substituting (94) into (82), we have:

$$\begin{aligned} v_{bat}[k] &= CA_0^k x[0] + C (qI - A_0)^{-1} Lv_{bat}[k] - C (qI - A_0)^{-1} L OCV[0] \mathbf{1}[k] + \\ &\quad + C (qI - A_0)^{-1} \frac{L}{C_0} q_{out}[k] + C (qI - A_0)^{-1} B_a i_{bat}[k] + \\ &\quad + OCV[0] \mathbf{1}[k] - \frac{1}{C_0} q_{out}[k] - R_0 i_{bat}[k] \\ &= CA_0^k x[0] + C (qI - A_0)^{-1} i_{bat}[k] B_a - i_{bat}[k] R_0 + \\ &\quad + C (qI - A_0)^{-1} v_{bat}[k] L + \mathbf{1}[k] OCV[0] - q_{out}[k] \frac{1}{C_0} - \\ &\quad - C (qI - A_0)^{-1} \mathbf{1}[k] L OCV[0] + C (qI - A_0)^{-1} q_{out}[k] \frac{L}{C_0} \end{aligned} \quad (96)$$

Defining

$$\begin{aligned}
i_{Fbat}[k] &:= (qI - A_0^T)^{-1} C^T i_{bat}[k], \\
v_{Fbat}[k] &:= (qI - A_0^T)^{-1} C^T v_{bat}[k], \\
\mathbf{1}_F[k] &:= (qI - A_0^T)^{-1} C^T \mathbf{1}[k], \\
q_{outF}[k] &:= (qI - A_0^T)^{-1} C^T q_{out}[k],
\end{aligned}$$

where $\mathbf{1}[k]$ is the unit step, we can rewrite (96) as

$$\begin{aligned}
v_{bat}[k] &= CA_0^k x[0] + i_{Fbat}[k]^T B_a - i_{bat}[k] R_0 + v_{Fbat}^T[k] L + \mathbf{1}[k] OCV[0] - \\
&\quad - q_{out}[k] \frac{1}{C_0} - \mathbf{1}_F^T[k] L OCV[0] + q_{outF}^T[k] \frac{L}{C_0}. \tag{97}
\end{aligned}$$

Defining

$$\begin{aligned}
\theta_A &:= x[0] \in \mathbb{R}^{n_x}, \\
\theta_B &:= B_a \in \mathbb{R}^{n_x}, \\
\theta_C &:= R_0 \in \mathbb{R}, \\
\theta_D &:= L \in \mathbb{R}^{n_x}, \\
\theta_E &:= OCV[0] \in \mathbb{R}, \\
\theta_F &:= \frac{1}{C_0} \in \mathbb{R}, \\
\theta_G &:= L OCV[0] \in \mathbb{R}^{n_x}, \\
\theta_H &:= \frac{L}{C_0} \in \mathbb{R}^{n_x}.
\end{aligned}$$

Observe that

$$\theta_G = \theta_D \theta_E, \tag{98}$$

$$\theta_H = \theta_D \theta_F. \tag{99}$$

Thence

$$\begin{aligned}
y[k] := v_{bat}[k] &= CA_0^k \theta_A + i_{Fbat}^T[k] \theta_B - i_{bat}[k] \theta_C + v_{Fbat}^T[k] \theta_D + \mathbf{1}[k] \theta_E \\
&\quad - q_{out}[k] \theta_F - \mathbf{1}_F^T[k] \theta_G + q_{outF}^T[k] \theta_H \\
&= \varphi_A[k] \theta_A + \varphi_B[k] \theta_B + \varphi_C[k] \theta_C + \varphi_D[k] \theta_D + \varphi_E[k] \theta_E \\
&\quad + \varphi_F[k] \theta_F + \varphi_G[k] \theta_G + \varphi_H[k] \theta_H \\
&= \varphi_1 \theta_1 \tag{100}
\end{aligned}$$

where

$$\begin{aligned}
\varphi_1 &:= [\varphi_A[k] \ \varphi_B[k] \ \varphi_C[k] \ \varphi_D[k] \ \varphi_E[k] \ \varphi_F[k] \ \varphi_G[k] \ \varphi_H[k]], \\
\theta_1 &:= [\theta_A^T \ \theta_B^T \ \theta_C \ \theta_D^T \ \theta_E \ \theta_F \ \theta_G^T \ \theta_H^T]^T,
\end{aligned}$$

with

$$\begin{aligned}
\varphi_A[k] &:= CA_0^k \in \mathbb{R}^{1 \times n_x}, \\
\varphi_B[k] &:= i_{Fbat}^T[k] \in \mathbb{R}^{1 \times n_x}, \\
\varphi_C[k] &:= -i_{bat} \in \mathbb{R}, \\
\varphi_D[k] &:= v_{Fbat}^T[k] \in \mathbb{R}^{1 \times n_x}, \\
\varphi_E[k] &:= \mathbf{1}[k] \in \mathbb{R}, \\
\varphi_F[k] &:= -q_{out}[k] \in \mathbb{R}, \\
\varphi_G[k] &:= -\mathbf{1}_F^T[k] \in \mathbb{R}^{1 \times n_x}, \\
\varphi_H[k] &:= q_{outF}^T[k] \in \mathbb{R}^{1 \times n_x}.
\end{aligned}$$

Given

$$Y_i := [y[1] \ \cdots \ y[N_i]]^T, \quad (101)$$

$$\Phi_i := \begin{bmatrix} \varphi_i[1] \\ \vdots \\ \varphi_i[N_i] \end{bmatrix} = [\Phi_A \ \Phi_B \ \Phi_C \ \Phi_D \ \Phi_E \ \Phi_F \ \Phi_G \ \Phi_H], \quad (102)$$

with $i = 1$ and the observer A_0 . The parameters can be found by minimising the cost function

$$J_i(\theta) = \frac{1}{2} (Y_i - \Phi_i \theta)^T (Y_i - \Phi_i \theta). \quad (103)$$

Taking into account restrictions (98) and (99), the unknown parameter vector becomes:

$$\Theta_1 := [\theta_A^T \ \theta_B^T \ \theta_C \ \theta_D^T \ \theta_E \ \theta_F]^T \quad (104)$$

and

$$\Phi_1 \theta_1 = [\Phi_A \ \Phi_B \ \Phi_C \ \Phi_D + \Phi_G \theta_E + \Phi_H \theta_F \ \Phi_E \ \Phi_F] \Theta_1 = \Psi_1 \Theta_1. \quad (105)$$

Hence

$$J_i(\theta) = V_i(\Theta) = \frac{1}{2} (Y_i - \Psi_i \Theta_i)^T (Y_i - \Psi_i \Theta_i) \quad (106)$$

and its minimum occurs when its gradient is zero:

$$\left[\frac{dV(\Theta_i)}{d\Theta_i} \right]^T = - \left(\Psi_i + \frac{d\Psi_i}{d\Theta_i} \Theta_i \right)^T (Y_i - \Psi_i \Theta_i) = 0 \quad (107)$$

where

$$\begin{aligned}
&\Psi_1 + \frac{d\Psi_1}{d\Theta_1} \Theta_1 = \\
&= [\Phi_A \ \Phi_B \ \Phi_C \ \Phi_D + \Phi_G \theta_E + \Phi_H \theta_F \ \Phi_E + \Phi_G \theta_D \ \Phi_F + \Phi_H \theta_D]
\end{aligned} \quad (108)$$

The minimum of $V_i(\Theta)$ can be found by a Jacobi method where each iteration is given by

$$\Theta_i^{(j)} = \left[\left(\Psi_i + \frac{d\Psi_i}{d\Theta_i} \Theta_i \right)^T \ \Psi_i \right]^{-1} \left(\Psi_i + \frac{d\Psi_i}{d\Theta_i} \Theta_i \right) \Big|_{\Theta = \Theta_i^{(j-1)}} Y_i. \quad (109)$$

The algorithm is initialised with

$$\Theta_i^{(0)} = \begin{bmatrix} I_{3n_x+3} & 0_{(3n_x+3) \times 2n_x} \end{bmatrix} \hat{\theta}_i, \quad (110)$$

where $\hat{\theta}$ is the least squares estimate

$$\hat{\theta}_i = (\Phi_i^T \Phi_i)^{-1} \Phi_i^T Y_i. \quad (111)$$

5.1.2 Remaining segments: Known initial OCV and initial state

When both $OCV[0]$ and $x[0]$ are known, equation (97) may be written as

$$\begin{aligned} v_{bat}[k] - OCV_0[k] - CA_0^k x[0] &= i_{Fbat}^T[k] B_a - i_{bat}[k] R_0 + v_{Fbat}^T[k] L - \\ &\quad - q_{out}[k] \frac{1}{C_0} - OCV_{0F}^T[k] L + q_{outF}[k] \frac{L}{C_0}. \end{aligned} \quad (112)$$

where

$$OCV_0[k] = \mathbf{1}[k] OCV[0] \quad (113)$$

$$OCV_{0F}[k] = \mathbf{1}_F[k] OCV[0] = (qI - A_0^T)^{-1} C^T \mathbf{1}[k] OCV[0]. \quad (114)$$

Defining

$$y[k] := v_{bat}[k] - OCV_0[k] - CA_0^k x[0], \quad (115)$$

and

$$\varphi_I := v_{Fbat}[k] - OCV_{0F}[k] \quad (116)$$

then

$$y[k] = \varphi_i[k] \theta_i, \quad (117)$$

with

$$\varphi_i[k] := [\varphi_B[k] \quad \varphi_C[k] \quad \varphi_I[k] \quad \varphi_F[k] \quad \varphi_H[k]] \quad (118)$$

$$\theta_i := [\theta_B^T \quad \theta_C \quad \theta_D^T \quad \theta_F \quad \theta_H^T]^T. \quad (119)$$

Given (101), the observer matrix A_0 and

$$\Phi_i = \begin{bmatrix} \varphi_i[1] \\ \vdots \\ \varphi_i[N_i] \end{bmatrix} = [\Phi_B \quad \Phi_C \quad \Phi_I \quad \Phi_F \quad \Phi_H], \quad (120)$$

the parameters may be found by minimising (101) with $i \neq 1$, taking into consideration restriction (99). Due to this restriction, the true unknown parameter vector is also redefined:

$$\Theta_i := [\theta_B^T \quad \theta_C \quad \theta_D^T \quad \theta_F] \quad (121)$$

and

$$\Phi_i \theta_i = [\Phi_B \quad \Phi_C \quad \Phi_I + \Phi_H \theta_F \quad \Phi_F] \Theta_i = \Psi_i \Theta_i. \quad (122)$$

As in the previous section, Θ_i is estimated by minimising $V_i(\Theta_i)$ in (106) using the Jacobi method in (109) where

$$\Psi_i + \frac{d\Psi_i}{d\Theta_i}\theta_i = [\Phi_B \quad \Phi_C \quad \Phi_I + \Phi_H\theta_F \quad \theta_F + \Phi_H\theta_D] \quad (123)$$

and considering the initial value:

$$\Theta_i^{(0)} = [I_{2n_x+2} \quad 0_{(2n_x+2) \times n_x}] \hat{\theta}_i, \quad (124)$$

where $\hat{\theta}_i$ given by (111).

5.1.3 Observer matrix

The estimators of Sections 5.1.1 and 5.1.2 assume the observer matrix A_0 to be known. Therefore, it must be defined before running the estimators. This matrix is in the companion form of the observable canonical realisation and is only subject to the stability constraint. However, it determines the accuracy of the estimator. Hence, a natural choice is to choose A_0 such that $V_i(\Theta_i)$ in (106) is minimised. This can be done using search or gradient methods. As in this work we only need to estimate models of order 1 and 2, we chose to use an intensive search method that consists in testing all matrices A_0 whose eigenvalues are in a predefined grid, and then choosing the one that leads to the smallest value of $V_i(\Theta_i)$. To preserve the physical meaning of the estimated models, all eigenvalues of the search grid have a positive real part since the cell's discrete-time models result from the sampling of continuous-time models.

6 CASE STUDY

The data has been obtained using the discharge board described in [12] controlled by an Arduino UNO platform. An INR18650 F1L Li-ion cell, with capacity of $3350mAh$, standard discharge constant current of $0.2C$ ($650mA$) and maximum discharge current of $1.5C$ ($4875mA$), was discharged with current pulses of 10 seconds with an amplitude of about $750mA$. The time-interval between pulses was also 10 seconds. Both, the battery current and voltage, were measured with a sampling period of 8ms.

The measurements were disturbed by noise. A signal to noise ratio (SNR) around 24dB was measured in the voltage measurements, whereas the current noise was filtered with the Kalman filter with *smooth* covariance reset described in [12]. The voltage was also filtered with the same filter to compute the Best Fit Rate (BFR) index (125) and to perform the Monte Carlo simulations described later in this section.

The first 50000 data points, corresponding to a time window of 6 minutes and 40 seconds, were used to estimate the parameters of the simplified Randles circuit with the LSE (72) in Subsection 4.3.1. In addition, two Thévenin models of orders 1 and 2, respectively, were estimated using the algorithms described in 5. In what follows, we denote by MRandles, M1 and M2 the estimated Randles model and Thévenin models of order 1 and 2, respectively. The Goodness of fit

of the models is evaluated by the BFR index:

$$BFR(W) = \left(1 - \frac{\|v_{bat}^0(W) - \hat{v}_{bat}(W)\|}{\|v_{bat}^0(W) - \bar{v}_{bat}^0(W)\|} \right) \times 100\%, \quad (125)$$

where W is the time window, $v_{bat}^0(W)$ the filtered voltage at the cell terminals in the time window W , $\bar{v}_{bat}^0(W)$ its mean value and $\hat{v}_{bat}(W)$ the simulated voltage. Table 1, displays the estimated parameters (in IS units),

Parameter	MRandles	M1	M2
$OCV(0)$ (Volt)	4.166	4.165	4.1633
C_0 (F)	4093.8	2439.3	2368.3
A_w	0.0047	—	—
R_1 (Ω)	—	0.0153	0.0183
C_1 (F)	—	531.69	211.17
R_2 (Ω)	—	—	0.0063
C_2 (F)	—	—	5.7168
R_b (Ω)	0.1205	0.1206	0.1202

while Figure 13 compares the first 250000 measured values of the battery voltage, corresponding to a time interval of 33 minutes and 20 seconds, with the voltages simulated by the estimated models within the window 100000 : 110000, and in the validation data set zoomed out.

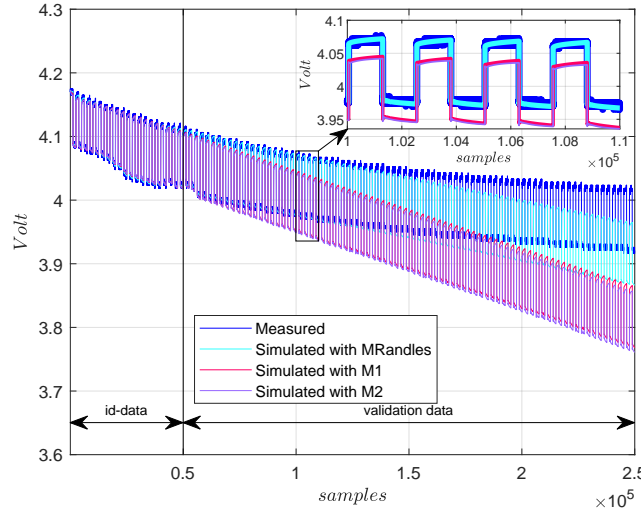


Figure 13: Measured and simulated voltage of the first 250000 points

This figure clearly shows that the MRandles model is accurate far beyond the window of the estimation data. The same is not true for the Thévenin models, whose accuracy is restricted to this window and its neighbourhood. This is

confirmed by Table 2 depicts the BFRs calculated in the time windows $W0 \equiv 1 : 50000$ (estimation data) $W1 \equiv 50001 : 100000$, $W2 \equiv 100001 : 150000$, $W3 \equiv 150001 : 200000$ and $W4 \equiv 200001 : 250000$, every with 50000 points (6 minutes and 40 seconds). Also from this table, one can see that the three models exhibit

Table 2: BFR indexes — First 250000 points of the discharge cycle

Model	W0	W1	W2	W3	W4
MRandles	94.51%	93.06%	86.10%	54.39%	7.24%
M1	93.56%	68.90%	4.50%	-83.91%	-184.53%
M2	93.06%	65.74%	-2.75%	-95.30%	-199.81%

a similar accuracy in the identification window (W0), although the MRandles model is slightly better. This model is also much more robust to SOC variation as it keeps good accuracy in the two windows subsequent to the identification data, while the accuracy of the M1 and M2 degrades significantly. To test the robustness of the proposed algorithm to noise, three Monte Carlo simulations were performed. Each simulation consists of 100 identification experiments with the filtered current as input and the filtered voltage disturbed by Gaussian white noise as output. The SNR was defined as the ratio between the filtered voltage peak to peak value and the noise standard deviation. It was of 20dB for the first simulation, 10dB for the second and 0dB for the third. Table 3 shows the mean values of the estimated model parameters with the respective standard deviations (in brackets), while Table 4 depicts the average BFRs and respective standard deviations (also in brackets). We can observe that even in extreme noise conditions (SNR=0dB) both the parameters and the BFRs in windows W0 and W1 did not suffer significant variations, denoting a high degree of noise immunity of the algorithm

Figure 13 and Table 2 show that an entire discharge cycle cannot be described by an LTI model. This is because the model parameters depend on SOC. To determine this dependence the discharge cycle was split into several segments, and an LTI Randles model was identified for each segment. In this way, we obtained an algorithm that identifies a piecewise LTI model capable of describing the entire discharge cycle. Moreover, since the OCV is a state of the model, it can be estimated by a suitable observer and its dependence on the SOC can be determined without performing a time consuming experiment. Figure 14 compares the measured battery voltage with the simulated by a piecewise LTI model with segments of 150000 data points identified by the algorithm. It also depicts the OCV estimated by the model. The overall BFR was 93.77% denoting

Table 3: Estimated parameters with different noise levels

SNR (dB)	OCV(0)(Volt)	A_w	C_0 (F)	R_b (Ω)
20	4.1625 (0.0005)	3987.3 (49.6735)	0.0041 (0.0001)	0.1177 (0.0001)
10	4.1625 (0.0015)	4009.4 (145.11)	0.0041 (0.0003)	0.1176 (0.0004)
0	4.1632 (0.0052)	4049.0 (491.30)	0.0042 (0.0010)	0.1176 (0.0014)

Table 4: BFR of the MRandles model for several noise levels

SNR (Db)	W0	W1	W2	W3	W4
20	95.13% (0.003%)	94.30% (0.14%)	83.94% (1.47%)	49.31% (2.66%)	-0.04% (3.69%)
10	95.07% (0.02%)	94.00% (0.54%)	84.24% (4.04%)	50.18% (7.60%)	1.21% 10.60%
0	94.60% (0.22%)	91.96% (2.60%)	80.10% (9.32%)	48.78% (22.93%)	0.23% (33.36%)

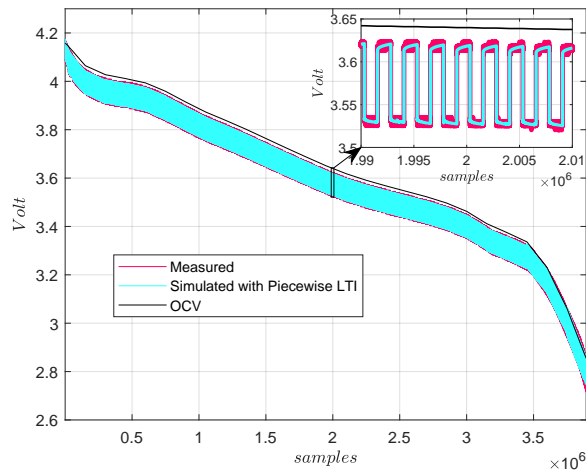


Figure 14: Discharge in the entire SOC

the model high accuracy.

References

- [1] G. Barbero, I. Lelidis, “Analysis of Warburg’s impedance and its equivalent electric circuits”, *Phys. Chem. Chem. Phys.*, 19(36), 24934–24944, 2017.
- [2] A. Baughman, M. Ferdowsi, “Battery charge equalisation-state of the art and future trends”, *SAE Transactions*, 905–910, 2005.
- [3] S. Buller *et al.*, ”Impedance-Based Simulation Models of Supercapacitors and Li-Ion Batteries for Power Electronic Applications”, in *IEEE Transactions on Industry Applications*, **41**, 742–747, 2005.
- [4] Z. Haizhou, “Modeling of lithium-ion battery for charging/ discharging characteristics based on circuit model” , *Int. J. of Online and Biomedical Engineering (iJOE)*, 13(06), 86–95 2017.
- [5] H. Hinz, “Comparison of lithium-ion battery models for simulating storage systems in distributed power generation”, *Inventions*, vol. 4(3), art. nr. 41, 2019.

- [6] Y. Jiang *et al.*, “Fractional-order autonomous circuits with order larger than one”, *Journal of Advanced Research*, 25, 217–225, 2020.
- [7] Y. Jin *et al.*, “Modeling and simulation of lithium-ion battery considering the effect of charge-discharge state”, *J. of Phys.: Conf. Ser.* **1907**, 1907 012003, 2021.
- [8] T. Katayama, *Subspace methods for system identification*. Springer-Verlag: London, 2005.
- [9] H. Lei, Y. Y. Han “The measurement and analysis for Open Circuit Voltage of Lithium-ion Battery”, *J. of Physics: Conf. Series* **1325** (1), 012173, 2019.
- [10] M. Li, “Li-ion dynamics and state of charge estimation”, *Renewable Energy*, 100, 44–52, 2017.
- [11] E. Locorotondo *et al.*, ”Modeling and simulation of constant phase element for battery electrochemical impedance spectroscopy”, in *Proc. 2019 IEEE 5th Int. Forum on Res. and Tech. for Society and Industry (RTSI)*, Firenze, Italy, Sept. 2019, 225–230.
- [12] P. Lopes dos Santos *et al.*, “Kalman filter for noise reduction of Li-Ion cell discharge current”, submitted to IFAC World Congress 2023, Yokohama, Japan, 2023, July 9-14.
- [13] P. Lopes dos Santos *et al.*, “Identification of optimal prediction error Thévenin models of Li-ion cells using the MOLI approach”, to be submitted arXiv.
- [14] B. Ospina Agudelo *et al.*, “A comparison of time-domain implementation methods for fractional-order battery impedance models”, *Energies*, 14(15), art. nr. 4415, 2021.
- [15] I. G. Pérez *et al.*, ”Modelling of Li-ion batteries dynamics using impedance spectroscopy and pulse fitting: EVs application,” *World Elect. Vehicle J.*, 2013, 6(3), 644-652.
- [16] G. L. Plett, “Battery management systems, Volume I: Battery modeling”, Artech House, 2015.
- [17] Podlubny, I. *et al.*, ”Analogue Realizations of Fractional-Order Controllers”, in *Nonlinear Dynamics*, **29**, 281–296, 2002.
- [18] A. Rahmoun, H. Biechl, “Modelling of Li-ion batteries using equivalent circuit diagrams”, *Przegląd Elektrotechniczny*, 88, 152–156, 2012
- [19] J. F. Reynaud *et al.*, “Active balancing circuit for advanced lithium-ion batteries used in photovoltaic application”, *Ren. en. & power qual. j.*, 1423–1428, 2011.
- [20] *Tutorial, Lithium-ion battery model*, PowerSIM, Oct. 2016. <https://powersimtech.com/resources/tutorials/lithium/ion-battery-model/>

- [21] K. Uddinet *et al.*, “Characterising lithium-Ion battery degradation through the identification and tracking of electrochemical battery model parameters”, *Batteries*, 2016, 2, 13.
- [22] S. Westerlund and L. Ekstam, ”Capacitor theory”, in *IEEE Transactions on Dielectrics and Electrical Insulation*, **1**(5), 826–839, 1994.
- [23] W. Heet *et al.*, “State of charge estimation for electric vehicle batteries using unscented Kalman filtering”, *Microelectronics Reliability*, 53 (6), 840–847, 2013.
- [24] M. Yu *et al.*, ”Fractional-order modeling of lithium-ion batteries using additive noise assisted modeling and correlative information criterion”, in *Journal of Advanced Research*, **25**, 49–56, 2020.
- [25] M. Zhang, X. Fan, “Review on the state of charge estimation methods for electric vehicle battery”, *World Electr. Veh. J*, 2020;, 11(1):23.
- [26] W. Zhou *et al.*, “Review on the battery model and SoC estimation method”, *Processes*, 9(9), art. nr. 1685, 2021.
- [27] L. Zhang *et al.*, ”A fractional-order model of lithium-ion batteries and multi-domain parameter identification method”, in *Journal of Energy Storage*, **50**, 104595, 2022.
- [28] L. Zhang *et al.*, ”A fractional-order model of lithium-ion batteries and multi-domain parameter identification method”, in *Journal of Energy Storage*, **50**, 104595, 2022.